Development of radiolabeled ligands targeting the Glu binding site of the NMDA receptor as potential imaging agents for brain

*Lucia Tamborini,[a] Ying Chen,[b] Catherine A. Foss,[b] Andrea Pinto,[a] Andrew G. Horti,[b] Stephen F. Traynelis,[c] Carlo De Micheli,[a] Ronnie C. Mease,[b] Kasper B. Hansen,[d]**

Paola Conti,[a] Martin G. Pomper[b]**

[a]Università degli Studi di Milano, Department of Pharmaceutical Sciences, Via Mangiagalli 25, 20133, Milano, Italy; [b]Russell H. Morgan Department of Radiology and Radiological Science, Johns Hopkins Medical School, Baltimore, MD, USA; [c]Department of Pharmacology, Emory University School of Medicine, Atlanta, GA, USA; [d]Department of Biomedical & Pharmaceutical Sciences, University of Montana, 32 Campus Drive, Missoula, MT 59812

KEYWORDS: NMDAR, glutamate, pyrazoline, PET, autoradiography

ABSTRACT

Abnormal activity of various *N*-methyl-D-aspartate receptor (NMDAR) subtypes has been implicated in a wide variety of neurological disorders such as Alzheimer's disease, schizophrenia and epilepsy. Imaging agents for PET and SPECT that target NMDARs in a subtype-selective fashion may enable better characterization of those disorders and enhance drug development.

Although such agents have long been sought, there is currently no validated imaging agent targeting NMDARs. Based on a pyrazoline derivative that demonstrated neuroprotective effects *in vivo*, we synthesized a series of *para*-substituted analogs and measured their affinities to various NMDAR subtypes in preparation for the corresponding radiolabeled imaging agents. Compounds **4a-c** and **4e** showed greater, nanomolar affinity for the GluN1/2A subtype versus GluN1/2B. Di-carbomethoxy (pro-drug) analogs of [$^{124/125}$I]**4d** and [^{11}C]**4e** (i.e., [$^{124/125}$I]**11d** and [^{11}C]**11e**) were generated and tested for NMDAR binding specificity in *ex vivo* autoradiography and brain biodistribution studies. Although NMDAR-specific binding could be demonstrated for [^{125}I]**11d** and [^{11}C]**11e** through autoradiography and biodistribution studies, imaging of neither [^{124}I]**11d** nor [^{11}C]**11e** could demonstrate brain penetration sufficient for detection by PET. Pyrazolines with higher affinity and lipophilicity will be required for this class of agents to serve as imaging agents at NMDARs.

Introduction

Glutamate-activated receptors belong to two families: ionotropic glutamate receptors (iGluRs) and metabotropic glutamate receptors (mGluRs). Within the class of ionotropic glutamate receptors, *N*-methyl-D-aspartate receptors (NMDARs) have been widely investigated for their involvement in neurodegenerative processes.[1] The majority of NMDA receptors are heterotetrameric assemblies of two glycine-binding GluN1 subunits and two glutamate binding GluN2 subunits, of which four types exist (GluN2A, B, C, D).[2] The various GluN2 subunits show differential temporal and spatial distribution in the central nervous system (CNS), and provide an opportunity to develop region-specific pharmacological regulation of NMDA receptor function using compounds selective for one individual GluN2 subunit.[3]

Unlike dopaminergic and serotonergic transmission, glutamatergic transmission has proven to be an elusive target for brain imaging, although several promising agents exist.[4,5] Positron emission tomography (PET) and single photon emission computed tomography (SPECT) imaging agents for glutamate receptors (GluRs) could be powerful tools for the evaluation of excitatory neurotransmission, the study of the pathophysiology of related neurological disorders, and the quantification of GluR drug occupancy *in vivo*. The strategy for the development of PET and SPECT probes for NMDA receptors involves the structural modification of NMDA receptor antagonists, including channel blockers, e.g. [^{11}C]ketamine, [^{18}F]fluoromemanthine and *N*-(1-naphthyl)-*N*-(3-[^{123}I]iodophenyl)-*N*-methylguanidine ([^{123}I]CNS-1261, **1**),[6] glycine site antagonists, e.g. 3-[3-(4-[^{11}C]methoxybenzyl)phenyl]-4-hydroxy-7-chloroquinolin-2(1H)-one ([^{11}C]L-703,717),[6] and GluN2B negative modulators, e.g. compound **2**,[6] (Figure 1).

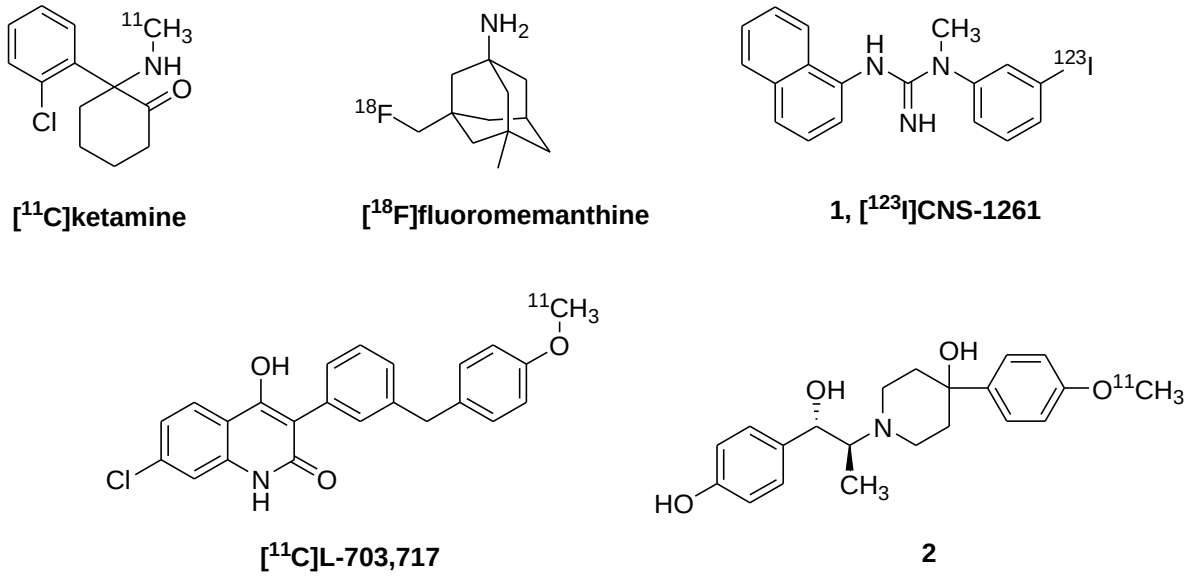

Figure 1. Structures of imaging agents for NMDA receptors.

For example, **1** is a channel-binding NMDA receptor radioligand for SPECT that has been used to study NMDA receptor function *in vivo* in humans.[7] While of high affinity and having been

tested in patients with schizophrenia, changes in **1** signal noted in affected individuals relative to controls, including those on clozapine, were small.[8] The results obtained with **1** proved sufficiently encouraging to pursue other compounds of its class for PET.[5] Nevertheless, most competitive antagonists of the glutamate binding site have shown low selectivity for NMDARs and poor blood-brain barrier (BBB) permeability, and at present there are no validated radioligands interacting with this region of the NMDARs.

In the last decade, we developed several new competitive NMDA receptor antagonists, as potential neuroprotective agents.[9] In particular, compound **3** (Figure 2) was highlighted for its promising pharmacological activity as a neuroprotective agent.[10] In binding assays, compound (5*S*,α*R*)-**3** showed nanomolar affinity for native receptors. Furthermore, preliminary evaluation of GluN2 subunit-selectivity suggested that the racemic mixture (±)-**3** displayed a preference for inhibition of NMDA receptors containing GluN2A or GluN2B subunits compared to receptors with GluN2C or GluN2D subunits.[10]

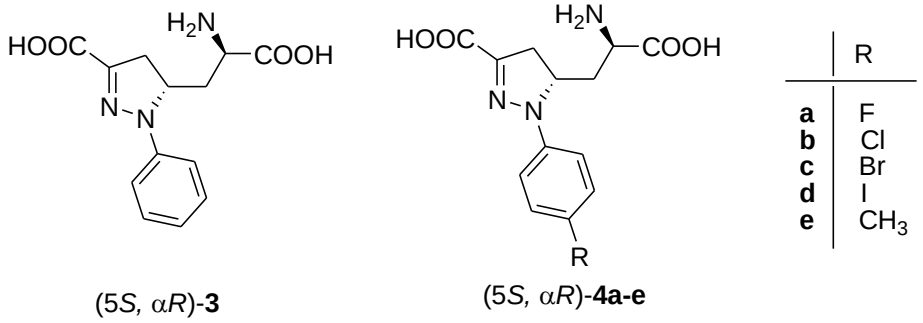

Figure 2. Structures of model and target compounds

Despite being a charged molecule, (±)-**3** displayed anticonvulsant activity after intra-peritoneal (ip) administration to mice, indicating the capacity to cross the intact BBB at the doses employed.[10]

Therefore, (5*S*,α*R*)-**3** appeared to us as a suitable tool to generate radiolabeled analogues for PET (or SPECT) imaging within the CNS.

Considering the molecular structure of (5*S*,α*R*)-**3**, we identified the *para* position of the aromatic ring as a suitable position for the insertion of a radiolabeled atom or group. We synthesized and pharmacologically tested several *p*-substituted-analogs, i.e. (5*S*,α*R*) **4a**-**e** (Figure 2), to measure how *para* substitution would affect the binding properties in terms of affinity and subtype selectivity. The *para* substituents included either a halogen (F, Br, I, compounds **4a, c, d**) or a methyl group (compound **4e**), that could be subsequently replaced by their radioactive counterpart, namely, ^{18}F, ^{76}Br, $^{124/125}$I, or ^{11}C. For a more thorough description of the structure-activity relationships (SARs), we included in this series also the *p*-Cl derivative (compound **4b**). The clogD and polar surface area (PSA) values of compounds **4a**-**e** were calculated as shown in Table 1. The negative clogD and high PSA values caution that, although the (5*S*,α*R*)-**3** possesses CNS activity, **4a**-**e** may not have sufficient BBB penetration when administered at the radiotracer level. Converting **4a**-**e** to the prodrugs **11a**-**e**, containing biologically cleavable methyl esters groups, significantly increased the clogD to positive values and also decreased PSA values, which may improve BBB penetration.

Table 1. Calculated CLogD and Polar Surface Areas

Compd.	**CLogD (pH 7.4)**	**PSA**
4a	-3.9	116.2
4b	-3.4	116.2
4c	-3.2	116.2

4d	-3.0	116.2
4e	-3.8	116.2
11a	0.1	94.2
11b	0.7	94.2
11c	0.9	94.2
11d	1.1	94.2
11e	0.3	94.2

[a]ACD/LogD Software, Advanced Chemistry Development, ACD/Labs Release 9.0, Product Version 9.1

Compounds **4d**, **11d** (prodrug of **4d**) and **11e** (prodrug of **4e**) were then prepared in radioactive form and submitted for biological investigation.

Results and discussion

Chemistry

Chloro-hydrazones **7a-e** were prepared by reacting the *p*-substituted anilines **5a-e** with methyl 2-chloro-3-oxobutanoate **6**, in the presence of sodium nitrite, 6 N HCl, sodium acetate and MeOH at 0 °C.[11] Chloro-hydrazones **7a-e** were treated with base to generate *in situ* the corresponding *N*-substituted-methoxycarbonylformonitrilimines that underwent 1,3-dipolar cycloaddition with suitably protected allylglycine **8** (Scheme 1). The cycloaddition reaction produced a mixture of stereoisomers **9** and **10** in an approximate 1:1 ratio, as estimated by ^{1}H NMR spectroscopy. Chromatographic separation of the two stereoisomers was unsuccessful at this stage; therefore, the mixture was treated with a 30% solution of trifluoroacetic acid (TFA) in dichloromethane to remove the *N*-Boc protecting group. The couples of amines **11a-e** and **12a-e** were easily separated by flash-chromatography. The desired stereoisomers **11a-e** were then converted into the final

amino acids **4a-e** through a three-step protection/deprotection strategy including a) *N*-Boc protection, b) hydrolysis of the two ester functions, and c) *N*-Boc deprotection, using standard procedures.

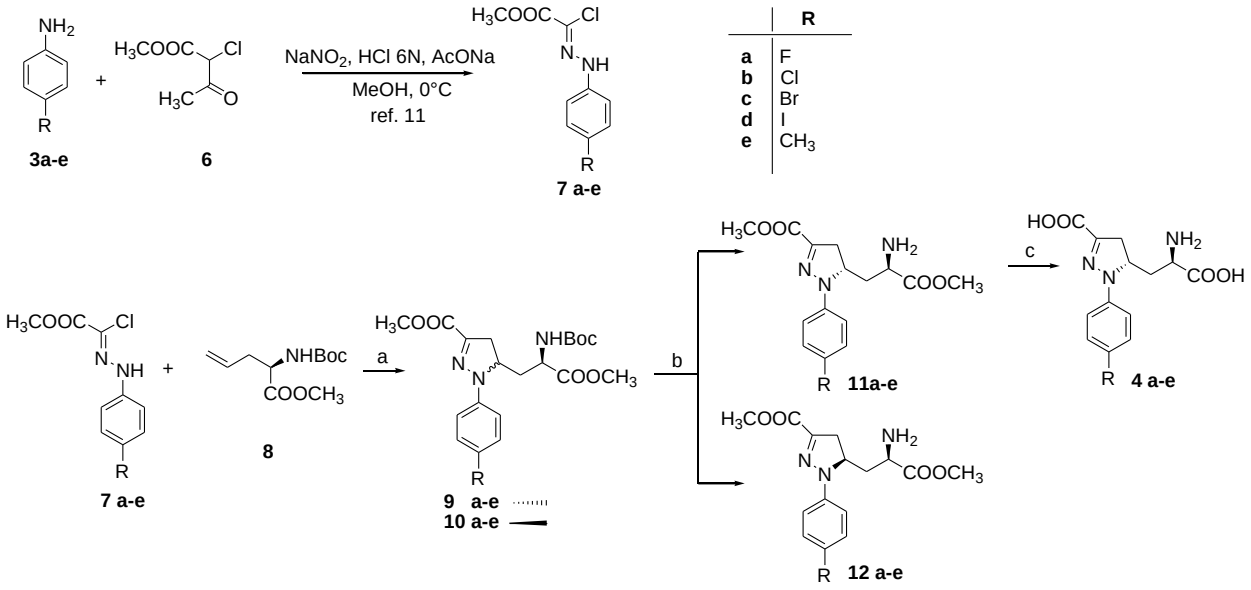

Scheme 1. a) $NaHCO_3$, EtOAc, Δ, 70-90% yield; b) i) 30% TFA, CH_2Cl_2; ii) flash chromatography; iii) Boc_2O, TEA, CH_2Cl_2, 78-87% yield after 3 steps; c) i) 1N NaOH, MeOH; ii) 30% TFA, CH_2Cl_2, 58-63% yield after 2 steps.

Pharmacology

Final amino acids **4a-e** were evaluated using two-electrode voltage-clamp electrophysiology at recombinant NMDA receptors expressed in *Xenopus* oocytes (Supplemental Figure 1 and Table 2).

Table 2. IC_{50} values for inhibition of current responses activated by 100 μM glycine and L-glutamate in oocytes expressing recombinant rat GluN1/2A, GluN1/2B, GluN1/2C, and GluN1/2D receptors. 10 μM L-glutamate was used for GluN1/2A, 3 μM L-glutamate for GluN1/2B and GluN1/2C, and 1 μM L-glutamate for GluN1/2D receptors. Ki values were estimated using the Cheng-Prusoff relationship with the following L-glutamate EC_{50} values: GluN1/2A 3.8 μM, GluN1/2B 1.9 μM, GluN1/2C 1.0 μM, and GluN1/2D 0.45 μM.[12,13] Hill slopes for the concentration-inhibition curves were 1.1 to 1.4, and 5-8 oocytes were recorded for each IC_{50} value using two-electrode voltage-clamp electrophysiology.

Cpd.	**GluN1/2A**		**GluN1/2B**		**GluN1/2C**		**GluN1/2D**	
	IC_{50} (nM)	**Est. K_i** (nM)	**IC_{50}** (nM)	**Est. K_i** (nM)	**IC_{50}** (nM)	**Est. K_i** (nM)	**IC_{50}** (nM)	**Est. K_i** (nM)
3	320 ±10	87±4	210±40	80±15	200±10	49±2	390±80	120±30
4a	160±10	43±2	860±10	330±40	920±20	230±10	920±20	290±10
4b	98±4	27±1	280±20	110±10	180±10	44±2	520±20	160±10
4c	91±4	25±1	250±20	94±7	190±10	47±3	630±40	200±10
4d	910±80	250±20	700±40	270±20	560±20	140±10	1.310±90	110±30
4e	180±10	48±3	690±50	250±20	380±20	96±5	1.420±60	440±20

The estimated K_i values for the model compound (5*S*,α*R*)-**3** at GluN1/2A and GluN1/2B receptor subtypes were 87 nM and 80 nM, respectively. Interestingly, we observed that the insertion of a substituent in the *para* position of compound (5*S*,α*R*)-**3** gave rise to compounds endowed with an increased affinity and selectivity for the GluN1/2A subtype versus GluN1/2B. In detail, by increasing the size of the substituent, the affinity for GluN1/2A increased up to a certain size (H < F, CH_3 < Cl, Br) and then it dropped with larger substituents such as I (compound **4d**). Notably,

the best selectivity GluN1/2A over GluN1/2B was obtained with the insertion of F (compound **4a**) or CH_3 (compound **4e**).

The estimated K_i values for compounds **4a** and **4e** were 7.6-fold and 5.3-fold higher, respectively, at GluN1/2B compared to at GluN1/2A (namely, the binding affinities were higher at GluN1/2A). Insertion of Cl (compound **4b**) resulted in an estimated K_i value that was 4.0-fold higher at GluN1/2B compared to at GluN1/2A. Among glutamate site competitive antagonists described to date, [(*R*)-[(*S*)-1-(4-bromophenyl)-ethylamino] - (2,3-dioxo- 1,2,3,4 - tetrahydroquinoxalin - 5 - yl) - methyl]-phosphonic acid (NVP-AAM077)[14] is generally considered to have the highest selectivity for GluN1/2A over GluN1/2B. However, its binding affinity is only modestly 5.2-fold higher for GluN1/2A (15 nM) compared to GluN1/2B (78 nM).[15] Thus, the 7.6-fold selectivity of compound **4a** for GluN1/2A over GluN1/2B represents a useful starting point for the development of a PET or SPECT ligand to image GluN1/2A receptors in the CNS. The ^{18}F-labeled analog of **4a** proved synthetically challenging requiring us to focus our radiosynthetic efforts on [^{11}C]**4e** and the corresponding radio-iodinated analogs for SPECT (^{125}I) and PET (^{124}I), [$^{125/124}$I]**4d**.

Radiochemistry

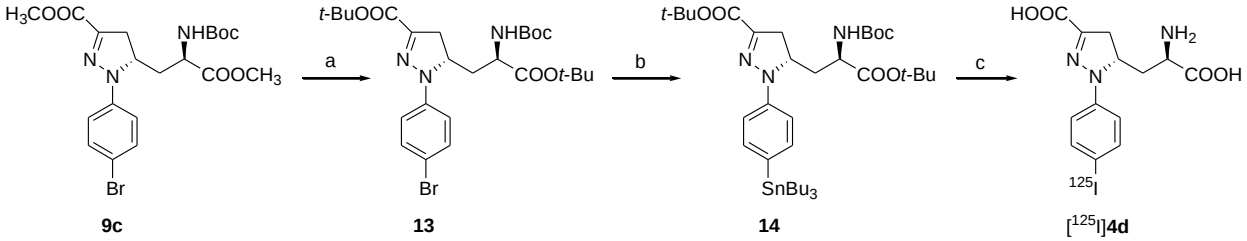

Scheme 2. a) i) 1N NaOH, MeOH, 95% yield; ii) TBTA, dry THF/CH_2Cl_2, 42% yield; b) Bu_6Sn_2, $Pd(PPh_3)_4$, toluene, 55% yield; c) i) AcOH, [^{125}]NaI, NCS, MeOH; ii) TFA/H_2O, 54% radiochemical yield.

The synthesis of the stannyl precursor **14** for the radioligand [^{125}I]**4d** is shown in Scheme 2. Aryl bromide **13**, prepared starting from **9c**, was treated with hexabutylditin in the presence of tetrakis(triphenylphosphine)palladium in toluene to give **14**. Radioiodination of **14** was carried out by treatment with [^{125}I]NaI in the presence of *N*-chlorosuccinimide followed by deprotection with TFA/H_2O to give [^{125}I]**4d**.

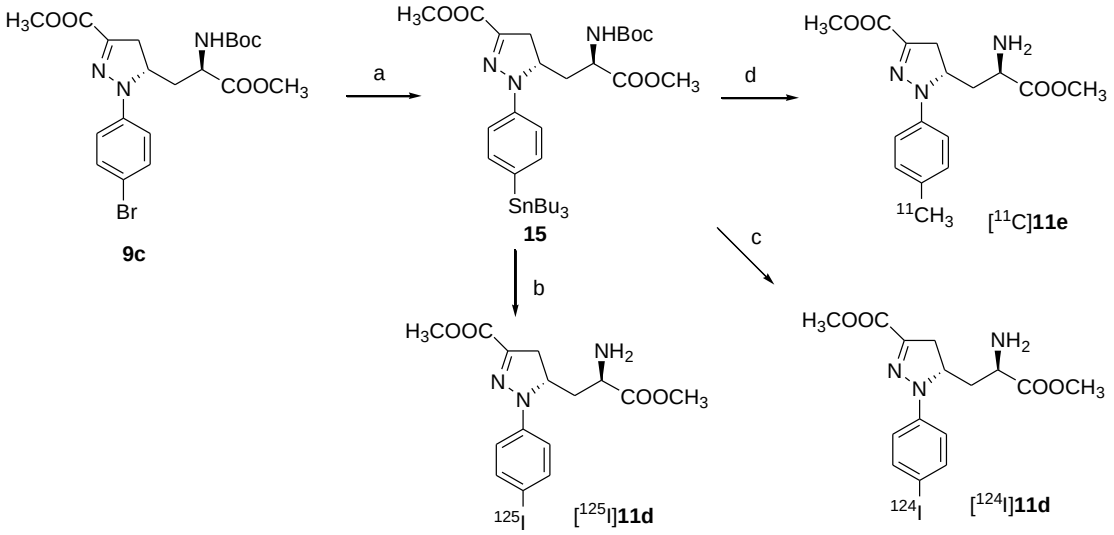

Scheme 3. a) Bu_6Sn_2, $Pd(PPh_3)_4$, toluene, 33% yield; b) i) AcOH, [^{125}]NaI, NCS, MeOH, radiochemical yield 58%; ii) TFA/H_2O; c) AcOH, [^{124}]NaI, NCS, MeOH; ii) TFA/H_2O, radiochemical yield 49%; d) i) [^{11}C]CH_3I, $Pd_2(dba)_3$, P(o-tol)$_3$, DMF; ii) TFA/H_2O, radiochemical yield 2-5%.

The synthesis of the stannyl precursor **15** for the radioligand [^{125}I]**11d**, [^{124}I]**11d** and [^{11}C]**11e** is shown in Scheme 3. Aryl bromide **9c** was treated with hexabutylditin in the presence of

tetrakis(triphenylphosphine)palladium in toluene to give **15**. Radioiodination of **15** was carried out by treatment with [^{125}I]NaI or [^{124}I]NaI in the presence of *N*-chlorosuccinimide followed by deprotection with TFA/H_2O to give [^{125}I]**11d** or [^{124}I]**11d**. [^{11}C]**11e** was prepared by Stille coupling reaction of **15** with [^{11}C]methyl iodide followed by deprotection with TFA/H_2O.

Autoradiography

Ex vivo autoradiography studies were conducted in female athymic nude mice with radiolabeled compounds [^{125}I]**4d** and prodrug [^{125}I]**11d** to qualitatively assess both the ability to cross the BBB as well as brain subregion selectivity. Each mouse was injected with radiotracer, allowed to undergo the indicated uptake time (Figure 3), sacrificed and then sections were cut and exposed to x-ray film. Compound [^{125}I]**4d** displayed no evidence of brain uptake (Figure 3A) while prodrug compound [^{125}I]**11d** displayed brain region-selective uptake (Figure 3B), particularly in cortex, hippocampus, thalamus (Supplemental Figure 2) and cerebellum with absence of uptake in caudate-putamen, which is consistent with the distribution of GluN1/2A subtype receptor mRNA expression.[16] Brain uptake of [^{125}I]**11d** exhibited high-contrast and region-specific retention but was low in absolute value as estimated by exposure time.

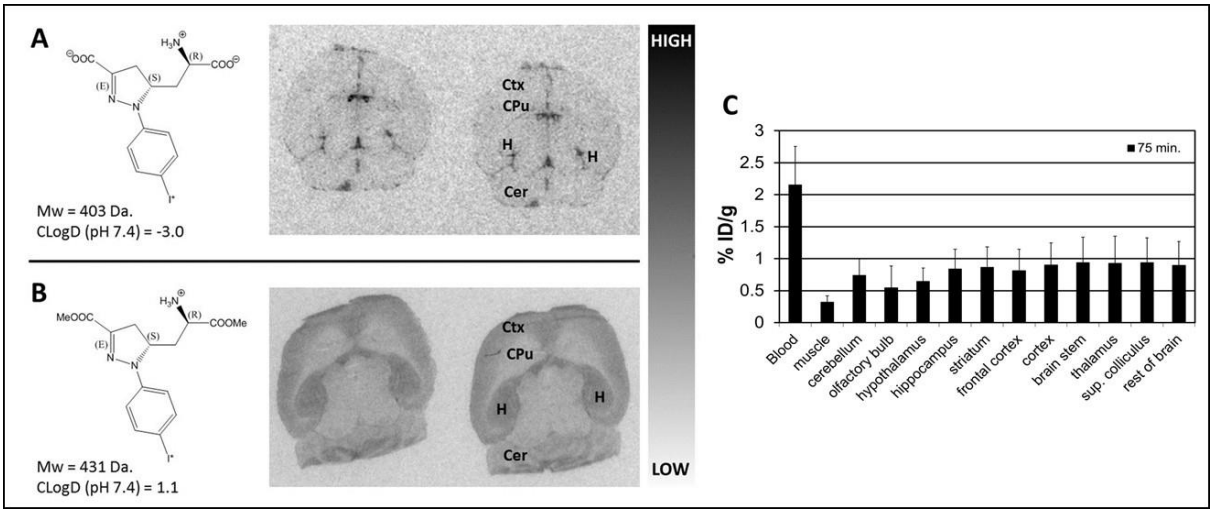

Figure 3. *In vivo* and *ex vivo* brain uptake and distribution of [^{125}I]**4d** and [^{125}I]**11d** prodrug in mice. A. *Ex vivo* autoradiography using [^{125}I]**4d** in serial brain sections following a 60 min conscious uptake. No evidence of radiotracer penetration into brain tissue is apparent. B. *Ex vivo* autoradiography using [^{125}I]**11d** prodrug in serial brain sections following a 40 min conscious uptake. Evidence of selective uptake in GluN2A subunit-rich regions is apparent including cortex (Ctx), hippocampus (H) and cerebellum (Cer). C. Ex vivo biodistribution of [^{124}I]**11d** in mice reflecting a 75 min uptake period confirms low overall brain uptake in the indicated tissue regions, indicating unsuitability for *in vivo* imaging.

Biodistribution

Ex vivo biodistribution in CD-1 mice was undertaken with prodrug compounds [^{124}I]**11d** and [^{11}C]**11e** to ascertain and quantify region-selective uptake. Compound [^{124}I]**11d** was injected into mice and allowed to undergo a 75 min biological uptake period to maximize *in vivo* prodrug cleavage and receptor binding. Figure 3C shows a graph of those uptake values as percentage of injected dose per gram of wet tissue (% ID/g) in selected regions. Uptake across regions was low and never exceeded 1% ID/g. *In vivo* PET imaging with this compound was also undertaken through 90 min and verified that brain uptake is below the threshold of detection for this modality (Supplemental Data).

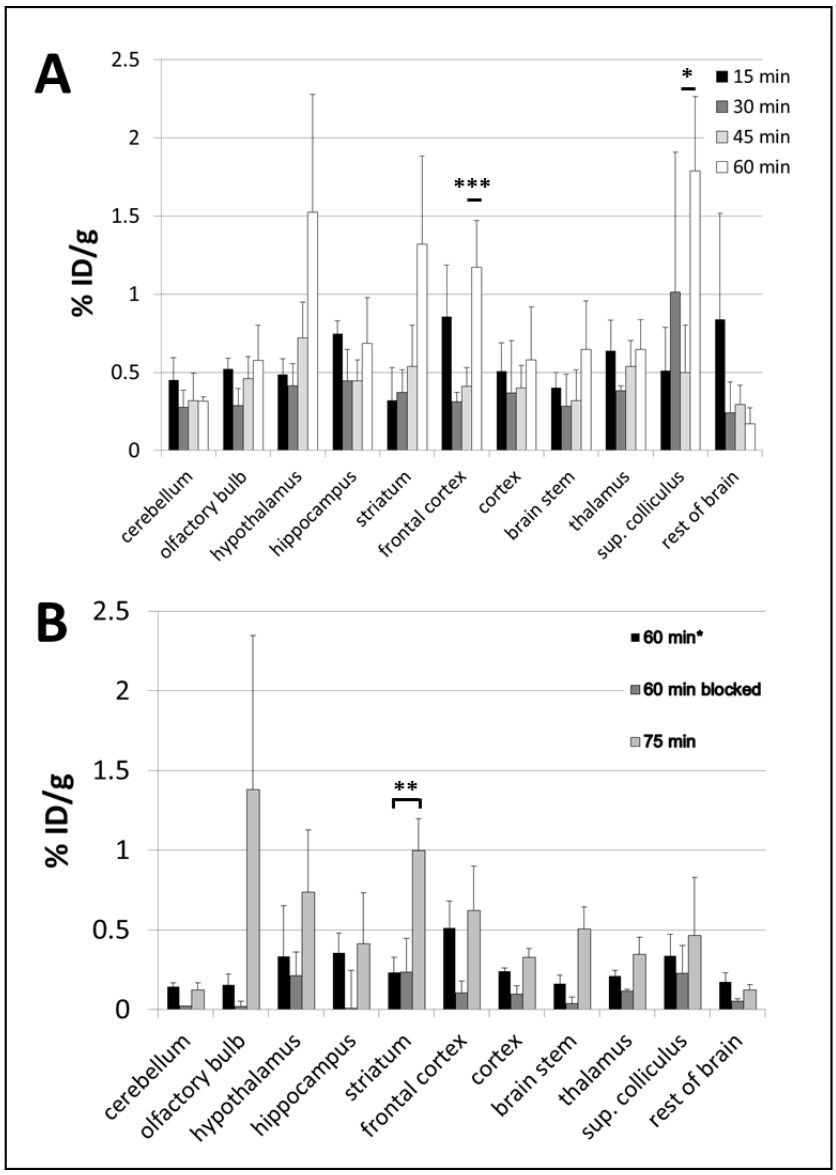

Figure 4. *Ex vivo brain biodistribution of [^{11}C]**11e** prodrug in mice.* **A**. Mice were injected with [^{11}C]**11e** and sacrificed at the indicated uptake times. The pattern of uptake in indicated brain tissues shows increasing radiotracer uptake over time in all regions except cerebellum and the remaining brain tissue following dissection. Significant radiotracer uptake was observed in frontal cortex (P = 0.004) and superior colliculus (P = 0.04) between 45 and 60 min of uptake. **B**. Autoblockade at 60 min after radiotracer injection compared with radiotracer alone at 60 and 75 min post-injection. Blockade was observed in cerebellum (85%), olfactory bulb (88%),

hippocampus (98%), frontal cortex (80%), cortex (60%), brainstem (77%), thalamus (45%) and in the remaining tissue (71%). Radiotracer-only uptake increased from 60-75 min in the same regions as in (A) where significance was only reached in striatum between 60 and 75 min of uptake (P = 0.009). Note: Specific radiotracer activity in (A) was 1,400 Ci/mmol while in (B) it was 11,500 Ci/mmol at the time of injection, which may account for differences in absolute % ID/g values.

Dimethyl ester [^{11}C]**11e**, for which GluN1/2A affinity of the free acid analog **4e** was found to be higher than that for **4d**, was also assayed by *ex vivo* biodistribution. Figure 4 shows the graph of uptake values from 15 min through 60 min of uptake (Figure 4A) as well as autoblockade at 60 min (Figure 4B) to verify radiotracer specificity. Figure 4A demonstrates radiotracer wash-in at 15 min followed by reduction at 30 min and then steady accumulation through 60 min, suggesting *in vivo* cleavage of the methyl esters and subsequent receptor binding over time. Figure 4B shows the effect of co-administration of 4.5 mg/kg of unlabeled compound **11e** with radiotracer at 60 min of uptake time as well as increasing uptake in radiotracer-only mice from 60 to 75 min, continuing the trend seen in Figure 4A.

Conclusion

Here we report the development of radiolabeled ligands [^{125}I]**4d**, [$^{124/125}$I]**11d** and [^{11}C]**11e** for *in vivo* targeting of NMDA receptors. [^{125}I]**4d** was not able to cross BBB when administered intravenously as a radiotracer. Applying a prodrug approach, both [$^{124/125}$I]**11d** and [^{11}C]**11e**, containing cleavable methyl ester groups, did demonstrate BBB penetration following intravenous administration and exhibited differentially selective brain sub-regional binding. [$^{124/125}$I]**11d** displayed an autoradiographic uptake profile consistent with the distribution of GluN2A subunits[16]

while *ex vivo* biodistribution of [^{11}C]**11e** suggested binding to both GluN1/2B and GluN1/2C, which accounts for both significant measured uptake in superior colliculus (GluN2C profile) and caudate-putamen (GluN2B profile). Compounds **11d** and **11e** differ only in the radiolabeled atom present in the same para position on the aryl ring where **11d** contains a large iodine atom and **11e** contains a smaller, less lipophilic methyl group. These differences may account for different murine *in vivo* GluN2 subunit binding selectivity, contrasting with the trends measured in *Xenopus* oocyte extracts in Table 2. It is also possible that the murine brain contains disparately distributed methyl esterase activity and/or each analog has a significantly different affinity for the esterase, efficient cleavage of which is necessary to convert prodrug analogs into the dicarboxylic acid species necessary to bind the targeted receptors (Supplemental Table 1).

Aside from the *ex vivo* evidence showing selective brain uptake for **11d** and **11e**, *in vivo* PET-CT imaging with [^{124}I]**11d** revealed no observable brain uptake (Supplemental Data). That was not unexpected when measured uptake values from *ex vivo* biodistribution studies revealed % ID/g values consistently below 1% ([^{124}I]**11d**, Figure 3C) or below 1.5% ID/g ([^{11}C]**11e**, Figure 4A, B). Although we previously showed that **3** could demonstrate neuroprotective properties,[10] further structure-activity relationships expanding upon this scaffold are necessary to identify compounds with sufficient affinity and suitable lipophilicity to serve as imaging agents for NMDARs in CNS. SAR studies will also be aimed at improving even further the specificity for the different subtypes of NMDA receptors. A potential utility for free-acids [^{124}I]**4d** and [^{11}C]**4e** would include imaging of NMDARs in peripheral neuroendocrine and neuroendocrine-like tumors, including melanomas, breast, small-cell lung cancer and castrate-resistant prostate cancers.[17] These free acids possess high affinity for their receptor subtypes (Table 2) and favorable clogD values (Table 1) for peripheral imaging.

Experimental

Solvents and chemicals purchased from commercial sources were of analytical grade or better and used without further purification. ^{1}H NMR and ^{13}C NMR spectra were recorded on a Bruker Ultrashield 400 MHz or on a Varian Mercury 300 (300 MHz) spectrometer. Chemical shifts (δ) are expressed in ppm, and coupling constants (*J*) are expressed in Hz. Rotary power determinations were carried out using a Jasco P-1010 spectropolarimeter, coupled with a Haake N3-B thermostat. TLC analyses were performed on commercial silica gel 60 F_{254} aluminum sheets; spots were further evidenced by spraying with a dilute alkaline potassium permanganate solution. Melting points were determined on a model B 540 Büchi apparatus and are uncorrected. MS analyses were performed on a Varian 320-MS triple quadrupole mass spectrometer with ESI source. Microanalyses (C, H, N) of new compounds were within ± 0.4 % of theoretical values. Chloro-hydrazones **7a-e** have been synthesized following a literature procedure.[11] HPLC purification of radiolabeled compounds was performed on Varian Prostar systems (Palo Alto, CA), equipped with a Varian ProStar 325 UV–Vis variable wavelength detector and a Bioscan Flow-count in-line radioactivity detector (Washington, DC). The specific radioactivity was calculated as the ratio of the radioactivity eluting at the retention time of product during the preparative HPLC purification to the mass corresponding to the area under the curve of the UV absorption.

Pharmacological studies

Two-electrode voltage-clamp recordings

Rat cDNAs for GluN1-1a (GenBank IDs U11418 and U08261), GluN2A (D13211), GluN2B (U11419), GluN2C (M91563), and GluN2D (L31611) were provided by Drs. S. Heinemann (Salk

Institute, La Jolla, CA), S. Nakanishi (Kyoto University, Kyoto, Japan), and P. Seeburg (University of Heidelberg, Heidelberg, Germany). The cDNA encoding rat GluN2B was modified without changing the amino acid sequence to remove a T7 RNA polymerase termination site located in the intracellular C-terminal domain as previously described.[18] For expression of NMDA receptors, cRNA for rat GluN1 (GluN1-1a splice variant), GluN2A, GluN2B, GluN2C, and GluN2D were prepared and injected into *Xenopus* oocytes as previously described.[19] The oocytes were surgically removed from mature female *Xenopus laevis* and provided by Xenopus1 (Dexter, MI). Recordings were performed 2-4 days after injection using two-electrode voltage-clamp electrophysiology in extracellular solution containing 115 mM NaCl, 2.5 mM KCl, 1.9 mM $BaCl_2$, and 10 mM HEPES (pH 7.6). The membrane potential was clamped at −40 mV. During recordings, 100 μM glycine was included in all agonist and/or antagonist applications. Electrophysiological data were acquired and analyzed as previously described.[19]

Native NMDA receptor binding assays

Affinities for native NMDA receptors in rat cortical synaptosomes were determined using 2 nM [^{3}H]CGP 39653, as previously described.[20]

Chemistry

General procedure for the cycloaddition reaction.

To a solution of (*R*)-methyl 2-(*tert*-butoxycarbonylamino)pent-4-enoate **8** (1.50 g, 6.54 mmol, 1.0 eq.) in EtOAc (25 mL), the appropriate chloro-hydrazone **7a-e** (9.81 mmol, 1.5 eq.) and solid $NaHCO_3$ (2.75 g, 32.7 mmol, 5 eq.) were added. The mixture was vigorously stirred for 24 h at 80 °C and the progress of the reaction was followed by TLC (cyclohexane/EtOAc 8:2). Water (5 mL)

was added and the organic layer was separated and dried over anhydrous Na_2SO_4. The crude material obtained after evaporation of the solvent was purified by column chromatography on silica gel to give an inseparable mixture of the two diastereoisomers **9a-e** and **10a-e** (Yield: 70-90%).

General procedure for the synthesis of compound 9a-e.

a) The mixture of diastereoisomers **9a-e** and **10a-e** (4.57 mmol, 1.0 eq.) was treated with a 30% CH_2Cl_2 solution of trifluoroacetic acid (3.5 mL, 10 eq.) at 0 °C. The solution was stirred at room temperature for 3 h and the reaction was followed by TLC (cyclohexane/EtOAc 8:2). A saturated solution of $NaHCO_3$ (50 mL) and CH_2Cl_2 (35 mL) were then added and the organic layer was separated, dried over anhydrous Na_2SO_4 and evaporated under reduced pressure. The crude material was purified on silica gel (cyclohexane/EtOAc 3:7) to give the amines **11a-e** and **12a-e** (Yield: 78-87%).

b) To a stirred solution of the amine **11a-e** (1.50 mmol, 1.0 eq) in CH_2Cl_2 (10 mL) cooled at 0 °C, triethylamine (2.25 mmol, 1.5 eq.) and a solution of di-*tert*-butyl dicarbonate (1.95 mmol, 1.3 eq.) in CH_2Cl_2 (3 mL) were added and the reaction mixture was stirred at room temperature overnight. The reaction was monitored by TLC (EtOAc). The solvent was evaporated under reduced pressure and the crude material was purified by column chromatography on silica gel (cyclohexane/EtOAc 8:2) to give compound **9a-e** in quantitative yield.

.

(*S*)-Methyl 5-((*R*)-2-(*tert*-butoxycarbonylamino)-3-methoxy-3-oxopropyl)-1-(4-fluorophenyl)-4,5-dihydro-1*H*-pyrazole-3-carboxylate (9a). Yield: 87%; yellow oil; R_f = 0.32

(cyclohexane/EtOAc 7:3); $[\alpha]_D^{20}$ = + 242.56 (c = 1.00; $CHCl_3$); ^{1}H NMR (300 MHz, $CDCl_3$): 1.45 (9H, s); 1.82–1.95 (1H, m); 1.95–2.05 (1H, m); 3.10 (1H, dd, *J* = 4.7, 17.8); 3.40 (1H, dd, *J* = 11.3, 17.8); 3.75 (3H, s); 3.90 (3H, s); 4.30–4.42 (1H, m); 4.62 (1H, dddd, *J* = 1.9, 4.7, 11.3, 11.3); 5.20 (1H, bd, *J* = 8.4); 6.98–7.06 (2H, m); 7.07–7.15 (2H, m); ^{13}C NMR (75 MHz, $CDCl_3$): 28.38; 35.09; 37.34; 50.50; 52.32; 52.86; 59.08; 80.73; 116.14 (d, *J* = 28.8); 116.24; 138.15; 138.68; 156.65; 157.85 (d, *J* = 300); 163.31; 172.35; $[M+H]^+$ = 424.2; anal. calcd for $C_{20}H_{26}FN_3O_6$: C, 56.73; H, 6.19; N, 9.92; found: C, 56.98; H, 6.31; N, 9.78.

(*S*)-Methyl 5-((*R*)-2-(*tert*-butoxycarbonylamino)-3-methoxy-3-oxopropyl)-1-(4-chlorophenyl)-4,5-dihydro-1*H*-pyrazole-3-carboxylate (9b). yellow oil; R_f = 0.15 (cyclohexane/EtOAc 8:2); $[\alpha]_D^{20}$ = + 230.37 (c = 1.00; $CHCl_3$); ^{1}H NMR (300 MHz, $CDCl_3$): 1.48 (9H, s); 1.80–1.95 (1H, m); 1.95–2.08 (1H, m); 3.10 (1H, dd, *J* = 4.7, 17.8); 3.40 (1H, dd, *J* = 11.3, 17.8); 3.75 (3H, s); 3.87 (3H, s); 4.30–4.42 (1H, m); 4.62 (1H, dddd, *J* = 2.8, 4.7, 11.3, 11.3); 5.22 (1H, bd, *J* = 7.5); 7.02–7.12 (2H, m); 7.20–7.28 (2H, m); ^{13}C NMR (75 MHz, $CDCl_3$): 28.50; 35.00; 37.48; 50.58; 52.49; 52.98; 58.76; 80.79; 116.07; 126.64; 129.47; 139.40; 140.49; 156.04; 163.31; 172.47; $[M+H]^+$ = 440.2; anal. calcd for $C_{20}H_{26}ClN_3O_6$: C, 54.61; H, 5.96; N, 9.55; found: C, 54.87; H, 6.12; N, 9.38.

(*S*)-Methyl 1-(4-bromophenyl)-5-((*R*)-2-(*tert*-butoxycarbonylamino)-3-methoxy-3-oxopropyl)-4,5-dihydro-1*H*-pyrazole-3-carboxylate (9c). yellow foam; crystallyzed from *n*-hexane; m.p. = 70–72 °C; R_f = 0.25 (cyclohexane/EtOAc 8:2); $[\alpha]_D^{20}$ = + 268.31 (c = 1.0; $CHCl_3$); ^{1}H NMR (300 MHz, $CDCl_3$): 1.48 (9H, s); 1.80–1.92 (1H, m); 2.02 (1H, ddd, *J* = 2.4, 10.6, 13.5); 3.09 (1H, dd, *J* = 4.7, 17.9); 3.38 (1H, dd, *J* = 11.7, 17.9); 3.73 (3H, s); 3.87 (3H, s); 4.30–4.42

(1H, m); 4.61 (1H, dddd, *J* = 2.4, 4.7, 11.7, 11.7); 5.26 (1H, bd, *J* = 8.5); 6.98–7.04 (2H, m); 7.34–7.41 (2H, m); ^{13}C NMR (75 MHz, $CDCl_3$): 28.53; 35.30; 37.58; 50.56; 52.53; 53.03; 58.69; 80.93; 114.12; 116.43; 132.42; 139.56; 140.91; 155.96; 163.28; 172.33; $[M+H]^+$ = 484.1; anal. calcd for $C_{20}H_{26}BrN_3O_6$: C, 49.60; H, 5.41; N, 8.68; found: C, 49.83; H, 5.58; N, 8.52.

(*S*)-Methyl 5-((*R*)-2-(*tert*-butoxycarbonylamino)-3-methoxy-3-oxopropyl)-1-(4-iodophenyl)-4,5-dihydro-1*H*-pyrazole-3-carboxylate (9d). yellow oil; R_f = 0.24 (cyclohexane/EtOAc 8:2); $[\alpha]_D^{20}$ = + 262.92 (c = 0.25; $CHCl_3$); ^{1}H NMR (300 MHz, $CDCl_3$): 1.48 (9H, s); 1.87 (1H, ddd, *J* = 3.5, 10.6, 11.1); 2.02 (1H, ddd, *J* = 2.4, 10.6, 13.5); 3.09 (1H, dd, *J* = 4.7, 17.9); 3.38 (1H, dd, *J* = 11.1, 17.9); 3.73 (3H, s); 3.87 (3H, s); 4.30–4.42 (1H, m); 4.61 (1H, dddd, *J* = 2.4, 4.7, 11.1, 11.1); 5.20 (1H, bd, *J* = 8.5); 6.85–6.95 (2H, m); 7.50–7.60 (2H, m); ^{13}C NMR (75 MHz, $CDCl_3$): 28.50; 35.25; 37.57; 50.67; 52.50; 52.99; 58.56; 80.90; 83.97; 116.89; 138.28; 139.69; 141.57; 155.97; 163.24; 172.32; $[M+H]^+$ = 532.2; anal. calcd for $C_{20}H_{26}IN_3O_6$: C, 45.21; H, 4.93; N, 7.91; found: C, 45.01; H, 4.9381; N, 8.01.

(*S*)-Methyl 5-((*R*)-2-(*tert*-butoxycarbonylamino)-3-methoxy-3-oxopropyl)-1-*p*-tolyl-4,5-dihydro-1*H*-pyrazole-3-carboxylate (9e). yellow foam; R_f = 0.42 (cyclohexane/EtOAc 7:3); $[\alpha]_D^{20}$ = + 326.90 (c = 1.00; $CHCl_3$); ^{1}H NMR (300 MHz, $CDCl_3$): 1.46 (9H, s); 1.80−1.93 (1H, m); 2.05 (1H, ddd, *J* = 2.2, 11.2, 13.5); 2.28 (3H, s); 3.05 (1H, dd, *J* = 4.9, 17.9); 3.36 (1H, dd, *J* = 11.2, 17.9); 3.70 (3H, s); 3.86 (3H, s); 4.30–4.42 (1H, m); 4.62 (1H, dddd, *J* = 2.2, 4.7, 11.2, 11.2); 5.20 (1H, bd, *J* = 8.5); 7.00–7.12 (4H, m); ^{13}C NMR (75 MHz, $CDCl_3$): 20.80, 28.50; 35.11; 37.19; 50.63; 52.30; 52.85; 58.92; 80.69; 115.19; 130.04; 131.36; 137.99; 139.52; 155.44; 163.55;

172.54; $[M+H]^+$ = 520.2; anal. calcd for $C_{21}H_{29}N_3O_6$: C, 60.13; H, 6.97; N, 10.02; found: C, 59.89; H, 6.77; N, 10.20.

General procedure for the synthesis of compound 4a-e.

a) Derivative **9a-e** (1.20 mmol, 1.0 eq.) was dissolved in MeOH (3.6 mL) and treated with 1 N aqueous NaOH (3.6 mL, 3.0 eq.). The disappearance of the starting material was monitored by TLC (cyclohexane/EtOAc 8:2). After evaporation of MeOH, the aqueous layer was washed with Et_2O (1 × 5 mL), made acidic with 2 N aqueous HCl and extracted with EtOAc (3 × 5 mL). The organic layer was dried over anhydrous Na_2SO_4 and, after evaporation of the solvent, the diacid derivative was obtained as a yellow solid. b) The diacid derivative (1.18 mmol, 1.0 eq.) was treated with a 30% CH_2Cl_2 solution of trifluoroacetic acid (11.8 mmol, 10 eq.) at 0 °C. The solution was stirred at room temperature for 3 h and the reaction was followed by TLC (CH_2Cl_2/MeOH 9:1 + 1% AcOH). The volatiles were removed under reduced pressure and the residue was crystallized to yield the final aminoacid **4a-e**.

(*S*)-5-((*R*)-2-Amino-2-carboxyethyl)-1-(4-fluorophenyl)-4,5-dihydro-1*H*-pyrazole-3-carboxylic acid (4a). Yield: 60%; yellow solid; m.p. = dec. T > 145 °C; R_f = 0.53 (BuOH/H_2O/AcOH 4:2:1); $[\alpha]_D^{20}$ = + 220.00 (c = 0.25; H_2O); ^{1}H NMR (300 MHZ, DMSO-*d6*): 1.75–1.85 (1H, m); 1.98–2.10 (1H, m); 2.98 (1H, dd, *J* = 3.8, 17.8); 3.20 (1H, dd, *J* = 12.2, 17.8); 3.62–3.75 (1H, m); 4.62–4.78 (1H, m); 7.08–7.25 (4H, m); ^{13}C NMR (75 MHz, DMSO-*d6*): 32.69; 37.35; 50.78; 58.79; 116.46; 116.49 (d, *J* = 22.2); 139.35; 141.30; 157.67 (d, *J* = 236); 164.39; 170.89; $[M+H]^+$ = 296.1; anal. calcd for $C_{13}H_{14}FN_3O_4$: C, 52.88; H, 4.78; N, 14.23; found: C, 53.02; H, 4.90; N, 14.11.

(*S*)-5-((*R*)-2-Amino-2-carboxyethyl)-1-(4-chlorophenyl)-4,5-dihydro-1*H*-pyrazole-3-carboxylic acid (4b). Yield: 63%; yellow solid; m.p. = dec. T > 175 °C; R_f = 0.58 (BuOH/H_2O/AcOH 4:2:1); $[\alpha]_D^{20}$ = + 393.2 (c = 0.20; DMSO); ^{1}H NMR (300 MHZ, DMSO-*d6*): 1.75–1.85 (1H, m); 1.95–2.10 (1H, m); 3.00 (1H, dd, *J* = 3.9, 18.3); 3.10 (1H, dd, *J* = 11.7, 18.3); 3.60–3.70 (1H, m); 4.60–4.78 (1H, m); 7.20 (2H, d, *J* = 7.8); 7.35 (2H, d, *J* = 7.8); ^{13}C NMR (75 MHz, DMSO-*d6*): 32.70; 37.38; 50.87; 58.49; 116.36; 124.79; 129.69; 141.62; 142.35; 164.41; 170.70; $[M+H]^+$ = 312.1; anal. calcd for $C_{13}H_{14}ClN_3O_4$: C, 50.09; H, 4.53; N, 13.48; found: C, 50.30; H, 4.62; N, 13.30.

(*S*)-5-((*R*)-2-amino-2-carboxyethyl)-1-(4-bromophenyl)-4,5-dihydro-1*H*-pyrazole-3-carboxylic acid (4c). Yield: 60%; yellow solid; m.p. = dec. T > 167 °C; R_f = 0.43 (BuOH/H_2O/AcOH 4:2:1); $[\alpha]_D^{20}$ = + 285.00 (c = 0.20; DMSO); ^{1}H NMR (300 MHZ, DMSO-*d6*): 1.70–1.85 (1H, m); 1.92–2.02 (1H, m); 2.99 (1H, dd, *J* = 4.1, 18.1); 3.19 (1H, dd, *J* = 11.6, 18.1); 3.55–3.65 (1H, m); 4.60–4.75 (1H, m); 7.15 (2H, d, *J* = 9.1); 7.41 (2H, d, *J* = 9.1); ^{13}C NMR (75 MHz, DMSO-*d6*): 32.74; 37.45; 50.94; 58.51; 112.65; 116.87; 132.55; 141.95; 142.26; 164.29; 170.57; $[M+H]^+$ = 355.8; anal. calcd for $C_{13}H_{14}BrN_3O_4$: C, 43.84; H, 3.96; N, 11.80; found: C, 43.67; H, 3.84; N, 11.92.

(*S*)-5-((*R*)-2-Amino-2-carboxyethyl)-1-(4-iodophenyl)-4,5-dihydro-1*H*-pyrazole-3-carboxylic acid (4d). Yield: 58%; yellow solid; m.p. = dec. T > 183 °C; R_f = 0.55 (BuOH/H_2O/AcOH 4:2:1); $[\alpha]_D^{20}$ = + 336.6 (c = 0.20; DMSO); ^{1}H NMR (300 MHZ, DMSO-*d6*): 1.70–1.82 (1H, m); 1.92–2.06 (1H, m); 2.97 (1H, dd, *J* = 3.8, 18.5); 3.18 (1H, dd, *J* = 11.1, 18.5);

3.58–3.70 (1H, m); 4.60–4.72 (1H, m); 7.02 (2H, *J* = 8.8); 7.57 (2H, *J* = 8.8); ^{13}C NMR (75 MHz, DMSO-*d6*): 32.66; 37.39; 50.77; 58.37; 83.74; 117.30; 138.29; 142.26; 142.39; 164.31; 170.59; $[M+H]^+$ = 404.1; anal. calcd for $C_{13}H_{14}IN_3O_4$: C, 38.73; H, 3.50; N, 10.42; found: C, 38.98; H, 3.60; N, 10.30.

(*S*)-5-((*R*)-2-Amino-2-carboxyethyl)-1-*p*-tolyl-4,5-dihydro-1*H*-pyrazole-3-carboxylic acid (4e). Yield: 62%; yellow solid; m.p. = dec. T > 198 °C; R_f = 0.60 (BuOH/H_2O/AcOH 4:2:1); $[\alpha]_D^{20}$ = + 335.00 (c = 0.10; H_2O); ^{1}H NMR (300 MHZ, DMSO-*d6*): 1.65–1.85 (1H, m); 1.90–2.10 (1H, m); 2.20 (3H, s); 2.95 (1H, dd, *J* = 4.4, 17.9); 3.15 (1H, dd, *J* = 11.3, 17.9); 3.35–3.45 (1H, m); 4.50–4.65 (1H, m); 7.02–7.18 (4H, m); ^{13}C NMR (75 MHz, DMSO-*d6*): 20.85; 33.18; 37.56; 51.53; 58.66; 114.89; 129.43; 130.22; 141.04; 142.78; 165.08; 170.67; $[M+H]^+$ = 292.1; anal. calcd for $C_{14}H_{17}N_3O_4$: C, 57.72; H, 5.88; N, 14.42; found: C, 58.00; H, 6.01; N, 14.23.

(*S*)-*tert*-Butyl 1-(4-bromophenyl)-5-((*R*)-3-*tert*-butoxy-2-(*tert*-butoxycarbonylamino)-3-oxopropyl)-4,5-dihydro-1*H*-pyrazole-3-carboxylate (13)

a) Derivative **9c** (290 mg, 0.60 mmol) was dissolved in MeOH (1.8 mL) and treated with 1 N aqueous NaOH (1.8 mL, 3.0 eq.). The disappearance of the starting material was monitored by TLC (cyclohexane/EtOAc 8:2). After evaporation of MeOH, the aqueous layer was washed with Et_2O (1 × 5 mL), made acidic with 2 N aqueous HCl and extracted with EtOAc (3 × 5 mL). The organic layer was dried over anhydrous Na_2SO_4 and, after evaporation of the solvent, the diacid derivative was obtained as a yellow solid (95% yield. b) The diacid intermediate (260 mg, 0.57 mmol) was dissolved in a mixture of dry THF (640 µL) and dry CH_2Cl_2 (2.40 mL) and *tert*-butyl 2,2,2-trichloroacetimidate (5.7 mmol, 1.02 mL) was added. The mixture was stirred overnight at

room temperature. A 5% solution of $NaHCO_3$ (50 mL) was added and the organic layer was separated. The aqueous phase was extracted with EtOAc (3 × 10 mL). The organic layer was dried over anhydrous Na_2SO_4 and, after evaporation of the solvent, the crude was purified by column chromatography (cyclohexane/EtOAc 9:1). Compound **13** was further purified by crystallization from *n*-hexane. Yield: 42%; R_f = 0.59 (cyclohexane/EtOAc 8:2); ^{1}H NMR (300 MHZ, $CDCl_3$): 1.42 (9H, s); 1.48 (9H, s); 1.58 (9H, s); 1.78–2.05 (2H, m); 3.02 (1H, dd, *J* = 4.8, 17.8); 3.38 (1H, dd, *J* = 11.9, 17.8); 4.12–4.25 (1H, m); 4.52–4.65 (1H, m); 5.25 (1H, bd, *J* = 8.5); 6.98–7.05 (2H, m); 7.32–7.42 (2H, m); anal. calcd for $C_{26}H_{38}BrN_3O_6$: C, 54.93; H, 6.74; N, 7.39; found: C, 55.16; H, 6.91; N, 7.27.

***tert*-Butyl (*S*)-5-((*R*)-3-(tert-butoxy)-2-((*tert*-butoxycarbonyl)amino)-3-oxopropyl)-1-(4-(tributylstannyl)phenyl)-4,5-dihydro-1*H*-pyrazole-3-carboxylate (14).**

Compound **13** (0.028 g, 0.049 mmol) and tetrakis(triphenylphosphine)palladium (0.010 g, 0.009 mmol) were placed in an oven-dried, resealable Schlenk tube. Toluene (1 mL) was added via syringe, followed by hexabutylditin (0.1 mL, 0.2 mmol). The tube was purged with nitrogen for 2 minutes and then sealed. Its contents were stirred for 4 hours at 100 ^{o}C, then cooled to room temperature and purified by flash chromatography (silica gel, EtOAc: hexanes = 1 : 4) to afford **14** (0.021 g, 55%). ^{1}H NMR (400 MHz, $CDCl_3$) δ 7.34 (2H, d, *J* = 8.0 Hz), 7.11 (2H, d, *J* = 8.0 Hz), 5.30 (1H, m), 4.59 (1H, m), 4.21 (1H, m), 3.31 (1H, m), 3.01 (1H, m), 2.01 (1H, m), 1.85 (1H, m), 1.43-1.54 (33H, m), 1.23-1.29 (6H, m), 0.97-1.02 (6H, m), 0.84-0.88 (9H, m).

(*S*)-5-((*R*)-2-amino-2-carboxyethyl)-1-(4-[^{125}I]iodophenyl)-4,5-dihydro-1*H*-pyrazole-3-carboxylic acid ([^{125}I]4d).

To a solution of **14** (0.5 mg, 0.64 μmol) in 0.1 mL of methanol was added 0.001 mL of acetic acid and 4.6 mCi [^{125}I]NaI solution, followed by *N*-chlorosuccinimide (0.005 mg, 0.037 μmol) in methanol. The reaction mixture was kept at room temperature for 20 minutes and then isolated by radio-HPLC (Econosil C18 10 μ, 250 mm × 4.6 mm, H_2O/CH_3CN/TFA = 70/30/0.1, 1 mL/min). The HPLC eluate at 26 min was collected and evaporated under vacuum. To it TFA/H_2O (95:5, 0.2 mL) was added. The mixture was heated at 40^{o}C for 10 min and isolated by radio-HPLC (Econosil C18 10 μ, 250 mm × 4.6 mm, H_2O/CH_3CN/TFA = 78/22/0.1, 1 mL/min, retention time: 17 min) to give [^{125}I]**4d**. The radiochemical yield was 54% and the specific activity was 1940 Ci/mmol.

Methyl (*S*)-5-((*R*)-2-((tert-butoxycarbonyl)amino)-3-methoxy-3-oxopropyl)-1-(4-(tributylstannyl)phenyl)-4,5-dihydro-1*H*-pyrazole-3-carboxylate (15).

Compound **9c** (0.050 g, 0.103 mmol) and tetrakis(triphenylphosphine)palladium (0.010 g, 0.009 mmol) were placed in an oven-dried, resealable Schlenk tube. Toluene (2 mL) was added via syringe, followed by hexabutylditin (0.3 mL, 0.6 mmol). The tube was purged with nitrogen for 2 min and then sealed. Its contents were stirred overnight at 95^{o}C, then cooled to room temperature and purified by flash chromatography (silica gel, EtOAc: hexanes = 1:3) to afford **15** (0.024 g, 33%). ^{1}H NMR (400 MHz, $CDCl_3$) δ 7.34 (2H, d, *J* = 8.0 Hz), 7.10 (2H, d, *J* = 8.0 Hz), 5.20 (1H, m), 4.64 (1H, m), 4.37 (1H, m), 3.85 (3H, s), 3.71 (3H, s), 3.36 (1H, m), 3.07 (1H, m), 2.06 (1H, m), 1.85 (1H, m), 1.44-1.58 (15H, m), 1.29-1.39 (6H, m), 0.98-1.02 (6H, m), 0.84-0.88 (9H, m).

Methyl (*S*)-5-((*R*)-2-amino-3-methoxy-3-oxopropyl)-1-(4-[^{125}I]iodophenyl)-4,5-dihydro-1*H*-pyrazole-3-carboxylate ([^{125}I]11d).

To a solution of **15** (0.5 mg, 0.72 μmol) in 0.1 mL of methanol was added 0.002 mL of acetic acid and 1 mCi [^{125}I]NaI solution, followed by *N*-chlorosuccinimide (0.02 mg, 0.15 μmol) in methanol. The reaction mixture was kept at room temperature for 20 minutes and then dried under vacuum. To it TFA/H_2O (95:5, 0.2 mL) was added. The mixture was kept at room temperature for 20 minutes and isolated by radio-HPLC (Econosil C18 10 μ, 250 mm × 4.6 mm, H_2O/CH_3CN/TFA = 70/30/0.1, 1 mL/min, retention time: 16 min) to give [^{125}I]**11d**. The radiochemical yield was 58% and the specific activity was 1,000 Ci/mmol.

Methyl (*S*)-5-((*R*)-2-amino-3-methoxy-3-oxopropyl)-1-(4-[^{124}I]iodophenyl)-4,5-dihydro-1*H*-pyrazole-3-carboxylate ([^{124}I]11d).

To a solution of **15** (0.01 mg, 0.014 μmol) in 0.1 mL of methanol was added 0.001 mL of acetic acid and 4.6 mCi [^{124}I]NaI solution, followed by *N*-chlorosuccinimide (0.02 mg, 0.15 μmol) in methanol. The reaction mixture was kept at room temperature for 20 minutes and then dried under nitrogen. To it TFA/H_2O (95:5, 0.2 mL) was added. After 20 min at 45^{o}C, the mixture was isolated by radio-HPLC (Phenomenex C18, 10 μ, 250 mm × 4.6 mm, H_2O/CH_3CN/TFA = 70/30/0.1, 1 mL/min, retention time: 16 min) to give [^{124}I]**11d**. The radiochemical yield was 49% and the specific activity was 13,000 Ci/mmol.

Methyl (*S*)-5-((*R*)-2-((tert-butoxycarbonyl)amino)-3-methoxy-3-oxopropyl)-1-(4-[^{11}C]methylphenyl)-4,5-dihydro-1*H*-pyrazole-3-carboxylate ([^{11}C]11e).

A reaction vial containing a solution of $Pd_2(dba)_3$ (1 mg) and tri(o-tolyl)phosphine (1.3 mg) in 0.1 mL DMF was purged with nitrogen for 2 minutes. To it compound **15** (1 mg in 0.1 mL DMF) was added. [^{11}C]MeI (prepared with GE 11C-methyl iodide radiosynthesis module and GE PETtrace cyclotron at Johns Hopkins PET center) was swept by argon flow into the reaction vial. After the radioactivity reached the plateau, the vial was heated at 90^{o}C for 7 min, 0.25 mL 95% TFA was added and mixture was heated at 90^{o}C for another 3 min. The reaction was diluted with 0.3 mL water and filtered through a 13 mm Teflon filter (0.45 micron) and purified by HPLC (Phenomenex Luna C18, 10 μ, 250 mm × 10 mm. H_2O/CH_3CN/TFA = 70/30/0.1, 8 mL/min, retention time 9-10 min) to give [^{11}C]**11e**. The radiochemical yield was 8-20 mCi starting from 400-500 mCi [^{11}C]MeI. Radiochemical purity was >99% and specific radioactivity was 6,000-23,000 Ci/mmol.

Animals. All animal studies were performed in compliance with a Johns Hopkins Animal Care and Use Committee approved protocol. Male CD-1 mice (7 weeks of age) were purchased from Charles River Laboratories (Frederick, MD) and were housed for several weeks in a specific pathogen free facility under a 12/12 light/dark cycle with free access to food and water *ad libitum*. Female athymic nude mice were purchased from Jackson Labs (Bar Harbor, ME) and housed under the same conditions. Rodent chow is Teklad 8604 (Harlan Labs, Frederick, MD).

Autoradiography. Athymic nude mice (n = 1 per compound) were injected with either 47 MBq (1.27 mCi, 1,940 Ci/mmol) of [^{125}I]**4d** for a 60 min conscious uptake or 9.1 MBq (246 μCi, 1,000

Ci/mmol) of [^{125}I]**11d** for a 40 min conscious uptake. No anesthetics were used. Following the indicated uptake times, the mice were sacrificed by cervical dislocation and their brains were rapidly harvested and frozen over dry ice. The brains were then sectioned using a cryotome (HM Microm 550, Microm Intl. GmbH, Waldorf, Germany) to 20 µm thickness and adhered to charged glass slides (VWR, Radnor, PA) before exposing them to x-ray film (Kodak Biomax XR, Sigma, St. Louis, MO). Brain sections containing compound [^{125}I]**4d** were exposed for 18 h while sections containing compound [^{125}I]**11d** were exposed for 24 h. Films were developed using a Kodak X-O-Mat film processor (Carestream, Rochester, NY). Exposures were digitized and displayed using an MCID Core system (MCID, Nottingham, UK) using the manufacturer's software.

Rodent biodistribution. [^{124}I]**11d**: Four male CD-1 mice were each injected intravenously with 1.85 MBq (50 µCi, 1,000 Ci/mmol) of radiotracer in 100 µL of PBS. They mice underwent a 75 min anesthetic-free uptake period prior to sacrifice by cervical dislocation. Selected tissues (blood, muscle, cerebellum, olfactory bulb, hypothalamus, hippocampus, caudate-putamen, frontal cortex, cortex, brain stem, thalamus, superior colliculus and rest of brain) were rapidly dissected, weighed and counted on a gamma counter (CS Compugamma 1282, LKB Wallac, Waverly, Vic) alongside diluted standard doses to obtain a percent injected dose per gram of wet tissue (% ID/g). Tissue uptake per region was averaged and graphed with standard deviation as indicated. [^{11}C]**11e**: kinetic biodistribution was carried out at 15, 30, 45 and 60 min post-injection (n = 4 mice per time point) following the I.V. injection of 3.7 MBq (100 µCi, 1,400 Ci/mmol) of radiotracer in 100 µL of PBS. Similarly, for the autoblockade study, 3.7 MBq (11,500 Ci/mmol) of radiotracer was injected alone or in combination with 4.5 mg/kg of unlabeled **11e** (n = 4/ group) in 100 µL of PBS. Time points

for the blockade study were 60 min (tracer-only and blocked) and 75 min (tracer-only). Tissues harvested and procedures were identical to those listed for [^{124}I]**11d**.

In vivo PET-CT imaging. Two female athymic nude mice underwent dynamic positron emission tomography (PET) imaging. The mice were maintained under anesthesia with 2.5% isoflurane in oxygen (2L/min) and positioned side-by-side in a small animal SuperArgus PET/CT system (Sedecal, Madrid, Spain). One mouse was administered 8.14 MBq (220 μCi) of ([^{124}I]**11d**) intravenously as a bolus. The other mouse received the same dose in addition to 150 mg/kg of ketamine. Dynamic PET imaging started simultaneously with dose administration and proceeded for 2 h, with the imaging field of view centered over the brain. A CT scan utilizing 360 projections at 60 keV was performed for anatomic co-registration purposes. Dynamic PET data were reconstructed using the manufacturer-provided 2D OSEM algorithm[21] and CT data were reconstructed with a manufacturer-provided standard filtered back-projection method. The PET reconstructed images were first co-registered with the CT using anatomic landmarks such as anterior eye socket to Harderian gland PET signal and displayed using AMIDE (http://amide.sourceforge.net/). Slices and 3D reconstructions were evaluated for brain uptake of radiotracer.

AUTHOR INFORMATION

Corresponding Authors

*For M.G.P: phone, (+1)410-955-2789; E-mail, mpomper@jhmi.edu

*For P.C.: phone, (+39)0250319329; E-mail, paola.conti@unimi.it

*For K.B.H.: phone (+1)406-243-4820; E-mail, kasper.hansen@mso.umt.edu

Notes

SFT is a co-founder of NeurOp Inc, is the PI on a research grant to Emory from Janssen, and is a paid consultant for NeurOp, Janssen, and Pfizer. The other authors declare no competing financial interest.

Supporting Information. Table S1 reporting the binding affinity for native NMDARs of compunds **4e** and **11e**; Figure S1 showing concentration-response data for **4a**, **4d**, **4e** at NMDA receptor subtypes; Figure S2 showing *ex vivo* autoradiography using [^{125}I]**11d** prodrug in brain sections. This material is available free of charge via the Internet at http://pubs.acs.org.

Author Contributions

The manuscript was written through contributions of all authors. All authors have given approval to the final version of the manuscript.

ACKNOWLEDGMENTS

The technical assistance of Birgitte Nielsen is gratefully acknowledged. This work was supported by National Institutes of Health (P20GM103546 and R01NS097536 to K.B.H.). A.P. acknowledges the financial support to the present research by the University of Milan (Piano di Sostegno alla Ricerca 2015/2017– Linea 2A).

ABBREVIATIONS USED: NMDAR, *N*-methyl-D-aspartate receptor; cLogD, calculated logarithm of distribution coefficient; EtOAc, ethyl acetate; AcOH, acetic acid; TEA, trimethylamine; Boc_2O, di-*tert*-butyl dicarbonate; TBTA, tris(benzyltriazolylmethyl)amine; % ID/g, percentage injected dose per gram; PET-CT imaging, positron emission tomography–computed tomography; HEPES, 4-(2-hydroxyethyl)-1-piperazine ethane sulfonic acid; cRNA, complementary ribonucleic acid; MBq, Megabecquerel.

References

1. Zhou, Q.; Sheng, M. NMDA receptors in nervous system diseases. *Neuropharmacology* **2013**, *74*, 69-75.

2. Buller, A. L.; Larson, H. C.; Schneider, B. E.; Beaton, J. A.; Morrisett, R. A.; Monaghan, D. T. The molecular basis of NMDA receptor subtypes: native receptor diversity is predicted by subunit composition. *J. Neurosci.* **1994**, *14*, 5471-5484.

3. Ogden, K. K.; Traynelis, S. F. New advances in NMDA receptor pharmacology. *Trends Pharmacol. Sci.* **2011**, *32*, 726–733.

4. Kassenbrock, A.; Vasdev, N.; Liang, S. H. Selected PET radioligands for ion channel linked neuroreceptor imaging: focus on GABA, NMDA and nACh receptors. *Curr. Top. Med. Chem.* **2016**, *16*, 1830-1842.

5. Naumiec, G. R.; Jenko, K. J.; Zoghbi, S. S.; Innis, R. B.; Cai, L.; Pike, V. W. N'-3-(Trifluoromethyl)phenyl Derivatives of *N*-aryl-*N*'-methylguanidines as prospective PET radioligands for the open channel of the *N*-methyl-D-aspartate (NMDA) receptor: synthesis and structure-affinity relationships. *J. Med. Chem.* **2015**, *58*, 9722-9730.

6. Fuchigami, T.; Nakayama, M. Yoshida. S. Development of PET and SPECT probes for glutamate receptors. *Sci. World J.*, **2015**, Article ID 716514. http://dx.doi.org/10.1155/2015/716514

7. J. Owens, A. A.; Tebbutt, A. L.; McGregor, A. L..; Kodama, K.; Magar, S. S.; Perlman, M. E.; Robins, D. J.; Durant, G. J.; McCulloch, J. Synthesis and binding characteristics of *N*-(1-

naphthyl)-*N*'-(3-[^{125}I]-iodophenyl)-*N*'-methylguanidine ([^{125}I]-CNS 1261): a potential SPECT agent for imaging NMDA receptor activation. *Nucl. Med. Biol.* **2000**, *27*, 557–564.

8. Bressan R. A.; Erlandsson, K.; Stone, J. M.; Mulligan, R. S.; Krystal, J. H.; Ell, P. J.; Pilowsky, L. S. Impact of schizophrenia and chronic antipsychotic treatment on [^{123}I]CNS-1261 binding to *N*-methyl-D-aspartate receptors *in vivo*. *Biol. Psychiatry* **2005**, *58*, 41-46.

9. (a) Conti, P.; Pinto, A., Tamborini, L.; Grazioso, G.; De Sarro, G.; Bräuner-Osborne, H.; Szabo, G.; Gábor Hársing, L.; De Micheli, C. Synthesis of conformationally constrained glutamic acid homologues and investigation of their pharmacological profiles. *ChemMedChem* **2007**, *2*, 1639-1647. (b) Conti, P.; De Amici, M.; Grazioso, G.; Roda, G.; Pinto, A.; Hansen, K. B.; Nielsen, B.; Madsen, U.; Bräuner-Osborne, H.; Egebjerg, J.; Vestri, V.; Pellegrini-Giampietro, D. E.; Sibille, P.; Acher, F. C.; De Micheli, C. Synthesis, binding affinity at glutamic acid receptors, neuroprotective effects, and molecular modeling investigation of novel dihydroisoxazole amino acids. *J. Med. Chem*. **2005**, *48*, 6315-6325. (c) Tamborini, L.; Pinto, A.; Mastronardi, F.; Iannuzzi, M. C.; Cullia, G.; Nielsen, B.; De Micheli, C.; Conti, P. 3-Carboxy-pyrazolinalanine as a new scaffold for developing potent and selective NMDA receptor antagonists. *Eur. J. Med. Chem.* **2013**, *68*, 33-37. (d) Conti, P.; De Amici, M.; Grazioso, G.; Roda, G.; Barberis Negra, F. F.; Nielsen, B.; Stensbøl, T. B.; Madsen, U.; Bräuner-Osborne, H.; Frydenvang, K.; De Sarro, G.; Toma, L.; De Micheli, C. Design, synthesis, and pharmacological characterization of novel, potent NMDA receptor antagonists. *J. Med. Chem.* **2004**, *47*, 6740-6748.

10. Conti, P.; Pinto, A.; Tamborini, L.; Madsen, U.; Nielsen, B.; Bräuner-Osborne, H.; Hansen, K. B.; Landucci, E.; Pellegrini Giampietro, D. E.; De Sarro, G.; Donato Di Paola, E.; De Micheli C. Novel 3-carboxy- and 3-phosphono-pyrazoline amino acids acting as potent and selective

NMDA antagonists: design, synthesis and pharmacological characterization. *ChemMedChem* **2010**, *5*, 1465-1475.

11. Pfefferkorn, J. A.; Choi, C.; Larsen, S. D.; Auerbach, B.; Hutchings, R.; Park, W.; Askew, V.; Dillon, L.; Hanselman, J. C.; Lin, Z.; Lu, G. H.; Robertson, A.; Sekerke, C.; Harris, M. S.; Pavlovsky, A.; Bainbridge, G.; Caspers, N.; Kowala, M.; Tait, B. D. Substituted pyrazoles as hepatoselective HMG-CoA reductase inhibitors: discovery of (3*R*,5*R*)-7-[2-(4-fluoro-phenyl)-4-isopropyl-5-(4-methyl-benzylcarbamoyl)-2H-pyrazol-3-yl]-3,5-dihydroxyheptanoic acid (PF-3052334) as a candidate for the treatment of hypercholesterolemia. *J. Med. Chem.* **2008**, *51*, 31-45.

12. Hansen, K. B.; Bräuner-Osborne, H.; Egebjerg, J. Pharmacological characterization of ligands at recombinant NMDA receptor subtypes by electrophysiological recordings and intracellular calcium measurements. *Comb. Chem. High Throughput Screen* **2008**, *11*, 304–315.

13. Cheng, Y.; Prusoff, W. H. Relationship between the Inhibition Constant (K1) and the Concentration of Inhibitor Which Causes 50 per Cent Inhibition (I50) of an Enzymatic Reaction. *Biochem. Pharmacol.* **1973**, *22*, 3099–3108.

14. Auberson, Y. P.; Allgeier, H.; Bischoff, S.; Lingenhoehl, K.; Moretti, R.; Schmutz, M. 5-Phosphonomethylquinoxalinediones as Competitive NMDA Receptor Antagonists with a Preference for the Human 1A/2A, rather than 1A/2B Receptor Composition. *Bioorg. Med. Chem. Lett.* **2002**, *12*, 1099–1102.

15. Frizelle, P. A.; Chen, P. E.; Wyllie, D. J. Equilibrium Constants for (R)-[(*S*)-1-(4-Bromo-Phenyl)-Ethylamino]-(2,3-Dioxo-1,2,3,4-Tetrahydroquinoxalin-5-Yl)-Methyl]-Phosphonic Acid (NVP-AAM077) Acting at Recombinant NR1/NR2A and NR1/NR2B N-Methyl-D-Aspartate

Receptors: Implications for Studies of Synaptic Transmission. *Mol. Pharmacol.* **2006**, *70*, 1022–1032.

16. Buller, A. L.; Larson, H. C.; Schneider, B. E.; Beaton, J. A.; Morrisett, R. A.; Monaghan, D. T. The molecular basis of NMDA receptor subtypes: native receptor diversity is predicted by subunit composition. *J. Neurosci.* **1994**, *14*, 5471-84.

17. (a) Akerman, B. L.; Allen, C. D.; Sylvain, N. P.; North, W. G. Abstract 3631: NMDA receptors as possible therapeutic targets for cancer. *Cancer Res* **2011**, *71*, 3631. (b) North, W. G.; Gao, G.; Jensen, A.; Memoli, V. A.; Du, J. NMDA receptors are expressed by small-cell lung cancer and are potential targets for effective treatment. *Clinical Pharmacology : Advances and Applications* **2010**, *2*, 31–40. (c) Song, Z.; He, C. D.; Liu, J.; Sun, C.; Lu, P.; Li, L.; Gao, L.; Zhang, Y.; Xu, Y.; Shan, L.; Liu, Y.; Zou, W.; Zhang, Y.; Gao, H.; Gao, W. Blocking glutamate-mediated signalling inhibits human melanoma growth and migration. *Exp Dermatol.* **2012**, *21,* 926-931.

18. Hansen, K. B.; Ogden, K. K.; Yuan, H.; Traynelis, S. F. Distinct Functional and Pharmacological Properties of Triheteromeric GluN1/GluN2A/GluN2B NMDA Receptors. *Neuron* **2014**, *81*, 1084–1096.

19. Hansen, K. B.; Tajima, N.; Risgaard, R.; Perszyk, R. E.; Jørgensen, L.; Vance, K. M.; Ogden, K. K.; Clausen, R. P.; Furukawa, H.; Traynelis, S. F. Structural Determinants of Agonist Efficacy at the Glutamate Binding Site of *N*-Methyl-D-Aspartate Receptors. *Mol. Pharmacol.* **2013**, *84*, 114–127.

20. Clausen, R. P.; Hansen, K. B.; Cali, P.; Nielsen, B.; Greenwood, J. R.; Begtrup, M. Egebjerg, J.; Bräuner-Osborne, H. The respective *N*-hydroxypyrazole analogues of the classical glutamate

receptor ligands ibotenic acid and (*RS*)-2-amino-2-(3-hydroxy-5-methyl-4-isoxazolyl)acetic acid. *Eur. J. Pharmacol.* **2004**, *499*, 35–44.

21. Jacobson, M.; Levkovitz, R.; Ben-Tal, A.; Thielemans, K.; Spinks, T.; Belluzzo, D.; Pagani, E.; Bettinardi, V.; Gilardi, M. C.; Zverovich, A.; Mitra, G. Enhanced 3D PETOSEM reconstruction using inter-update Metz filtering. *Phys Med Biol.* **2000**, *45*, 2417–2439.

Table of Contents